RESEARCH ARTICLE

WILEY

Celiac disease-associated *Neisseria flavescens* decreases mitochondrial respiration in CaCo-2 epithelial cells: Impact of *Lactobacillus paracasei* CBA L74 on bacterial-induced cellular imbalance

Giuseppe Labruna[1] [ORCID] | Merlin Nanayakkara[2] | Chiara Pagliuca[3] | Marcella Nunziato[3,4] | Laura Iaffaldano[4] | Valeria D'Argenio[3,4,5] | Roberta Colicchio[3] | Andrea L. Budelli[6] | Roberto Nigro[7] | Paola Salvatore[3] | Maria Vittoria Barone[2] | Lucia Sacchetti[4,5]

[1] IRCCS (Istituto di Ricovero e Cura a Carattere Scientifico) SDN, Naples, Italy

[2] Dipartimento di Scienze Mediche Traslazionali and European Laboratory for the Investigation of Food Induced Disease (ELFID), Università degli Studi di Napoli Federico II, Naples, Italy

[3] Dipartimento di Medicina Molecolare e Biotecnologie Mediche, Università degli Studi di Napoli Federico II, Naples, Italy

[4] CEINGE-Biotecnologie Avanzate SCarl, Naples, Italy

[5] Task Force on Microbiome Studies, Università degli Studi di Napoli Federico II and CEINGE-Biotecnologie Avanzate SCarl, Naples, Italy

[6] Kraft Heinz Innovation Center, Nijmegen, Netherlands

[7] Dipartimento di Ingegneria Chimica, dei Materiali e della Produzione Industriale, Università di Napoli Federico II, Naples, Italy

Correspondence
Maria Vittoria Barone, Dipartimento di Scienze Mediche Traslazionali, Università degli Studi di Napoli Federico II, Via S. Pansini 5, Naples 80131, Italy.
Email: mv.barone@unina.it

Lucia Sacchetti, CEINGE-Biotecnologie Avanzate SCarl, Via G. Salvatore 486, Naples 80145, Italy.
Email: sacchett@unina.it

Abstract

We previously identified a *Neisseria flavescens* strain in the duodenum of celiac disease (CD) patients that induced immune inflammation in ex vivo duodenal mucosal explants and in CaCo-2 cells. We also found that vesicular trafficking was delayed after the CD-immunogenic P31-43 gliadin peptide-entered CaCo-2 cells and that *Lactobacillus paracasei* CBA L74 (*L. paracasei*-CBA) supernatant reduced peptide entry. In this study, we evaluated if metabolism and trafficking was altered in CD-*N. flavescens*-infected CaCo-2 cells and if any alteration could be mitigated by pretreating cells with *L. paracasei*-CBA supernatant, despite the presence of P31-43. We measured CaCo-2 bioenergetics by an extracellular flux analyser, *N. flavescens* and P31-43 intracellular trafficking by immunofluorescence, cellular stress by TBARS assay, and ATP by bioluminescence. We found that CD-*N. flavescens* colocalised more than control *N. flavescens* with early endocytic vesicles and more escaped autophagy thereby surviving longer in infected cells. P31-43 increased colocalisation of *N. flavescens* with early vesicles. Mitochondrial respiration was lower ($P < .05$) in CD-*N. flavescens*-infected cells versus not-treated CaCo-2 cells, whereas pretreatment with *L. paracasei*-CBA reduced CD-*N. flavescens* viability and improved cell bioenergetics and trafficking. In conclusion, CD-*N. flavescens* induces metabolic imbalance in CaCo-2 cells, and the *L. paracasei*-CBA probiotic could be used to correct CD-associated dysbiosis.

KEYWORDS

CaCo-2 cells, celiac disease, *L. paracasei* CBA L74 probiotic, *Neisseria flavescens*, P31-43 gliadin peptide

Giuseppe Labruna and Merlin Nanayakkara contributed equally to the paper.

1 | INTRODUCTION

Microbial dysbiosis has been identified in patients with active celiac disease (CD) (Girbovan, Sur, Samasca, & Lupan, 2017; Kho & Lal, 2018). Using 16S rRNA analysis of duodenal and oropharyngeal samples from CD patients and control subjects (Ctr), we previously identified a peculiar *Neisseria flavescens* strain in adults affected by CD (D'Argenio et al., 2016; Iaffaldano et al., 2018). This bacterial strain, isolated from the above samples, induced an immune-inflammatory response in human and murine dendritic cells, in CaCo-2 cells, and in ex vivo duodenal mucosal explants of Ctr subjects, thereby suggesting that it could play a role in CD (D'Argenio et al., 2016). Whole-genome shotgun sequencing revealed alterations in the iron acquisition system, particularly in the haemoglobin receptor, neisserial haptoglobin-haemoglobin A/B, and transferrin A/B binding protein genes in the CD associated but not in Ctr-*N. flavescens* isolates (D'Argenio et al., 2016). Furthermore, intracellular trafficking between CD-*N. flavescens* and Ctr-*N. flavescens* isolates was delayed in CaCo-2 cells at the late lysosomal compartment (D'Argenio et al., 2016). Interestingly, delay of vesicular trafficking has also been reported after the CD-immunogenic P31-43 gliadin peptide entered CaCo-2 cells (Barone et al., 2010). CD is an autoimmune disorder caused by the loss of oral tolerance to gluten, in which changes of mucosal histology results from a Th1 response to certain gliadin peptides (e.g., the 33-mer A-gliadin peptide) presented by human leucocyte antigen-DQ2 or 8 (Sollid, 2000) and activation of innate immune pathways. Both the 33-mer and 25-mer (P31-55), which contain peptides P57-68 and P31-43, respectively, are very resistant to hydrolysis by gastric, pancreatic, and intestinal proteases. Thus, these peptides are active in vivo in the celiac intestine after gluten ingestion (Comino et al., 2012; Marsh, 1992; Shan et al., 2002). The mechanisms by which P31-43 might induce the innate immune response and enterocyte proliferation have been attributed to its effect on the endocytic compartment (Barone, Troncone, & Auricchio, 2014; Barone & Zimmer, 2016). In both celiac enterocytes and CaCo-2 cells, P31-43 localises to the early endosomes and delays vesicular trafficking (Barone et al., 2007, 2010; Barone & Zimmer, 2016). In detail, P31-43 shares sequence similarity with a region of growth factor-regulated tyrosine kinase substrate (HGS), the latter is located on the membranes of early endocytic vesicles and is a key molecule involved in regulating endocytic maturation (Barone et al., 2010). In CaCo-2 cells, P31-43 interferes with the correct localisation of HGS in early endosomes thereby delaying maturation of endocytic vesicles (Barone et al., 2010). Thus, P31-43 induces two important effects: (a) It delays endocytic maturation, and (b) it alters the recycling pathway.

Furthermore, low levels of *Lactobacilli* are one of the most consistent findings in the microbiomes of adults and children with active CD (D'Argenio et al., 2016; Di Cagno et al., 2011; Nadal, Donat, Ribes-Koninckx, Calabuig, & Sanz, 2007; Nistal et al., 2012). In addition, pretreatment of CaCo-2 cells with *Lactobacillus paracasei* CBA L74 supernatant (*L. paracasei*-CBA) reduced the entry of gliadin peptides in the cell, thereby decreasing their toxicity (Sarno et al., 2014).

In this scenario, we evaluated (a) if parallel to the inflammatory response, CD-*N. flavescens*-associated dysbiosis induces changes in CaCo-2 bioenergetics (measured by extracellular flux analyser: XF), thereby concurring to exacerbate the epithelial intestinal cell malfunction; (b) if the immunogenic P31-43 peptide interferes with the intracellular CD-*N. flavescens* pathway; and (c) if pretreatment of CaCo-2 cells with the *L. paracasei*-CBA supernatant could mitigate any of the effects exerted by CD-*N. flavescens*-associated dysbiosis on the CaCo-2 cells, notwithstanding the presence of the P31-43 peptide.

2 | RESULTS

2.1 | CD-*N. flavescens* and Ctr-*N. flavescens* localisation in the early, late, and autophagosomal vesicular compartments

We previously reported preliminary data showing that intracellular trafficking of CD-*N. flavescens* differs from that of Ctr-*N. flavescens* in CaCo-2 cells (D'Argenio et al., 2016). One of the aims of the present study was to verify and extend the intracellular trafficking of *N. flavescens*. To this aim, we investigated the localisation of CD-*N. flavescens* and Ctr-*N. flavescens* in the early, late, and autophagosomal compartments of CaCo-2 cells by immunofluorescence. We found that colocalisation of CD-*N. flavescens* and early endosome antigen 1 (EEA1), a marker of the early endocytic compartment, was significantly greater than that of Ctr-*N. flavescens* ($P < .0001$; Figure 1). Notably, significantly ($P < .01$) fewer CD-*N. flavescens* bacteria than Ctr-*N. flavescens* bacteria localised to the late anti-lysosomal-associated membrane protein-2 (LAMP-2) positive vesicles (Figure S1), which is in line with our previous finding (D'Argenio et al., 2016). Furthermore, using the microtubule-associated proteins 1A/1B light chain 3B (LC3) vesicle marker, we investigated the localisation of CD-*N. flavescens* and Ctr-*N. flavescens* bacteria in the autophagosomal compartment using immunofluorescence. As shown in Figure 2, CD-*N. flavescens* and LC3 colocalisation was significantly lower ($P < .01$) than that of Ctr-*N. flavescens*. Our data indicate that, unlike Ctr-*N. flavescens*, CD-*N. flavescens* preferentially localised to the early vesicular compartment and was able to elude the autophagosomal compartment.

2.2 | Effect of the P31-43 gliadin peptide on the localisation of CD-*N. flavescens* and Ctr-*N. flavescens* in the early, late, and autophagosomal vesicular compartments

To determine if and how the P31-43 gliadin peptide interferes with bacterial endocytosis, we infected CaCo-2 cells with CD-*N. flavescens* and Ctr-*N. flavescens* and treated them with the toxic P31-43 peptide. We used this gliadin peptide for two reasons: (a) It is resistant to intestinal endopeptidases and is thus active in the intestinal mucosa (Nanayakkara et al., 2018), and (b) it delays vesicular trafficking in intestinal epithelial cells (Barone et al., 2007). As shown in Figure 3a, b, P31-43 significantly decreased ($P < .05$) the colocalisation of CD-*N. flavescens* and Ctr-*N. flavescens* in the late compartment and
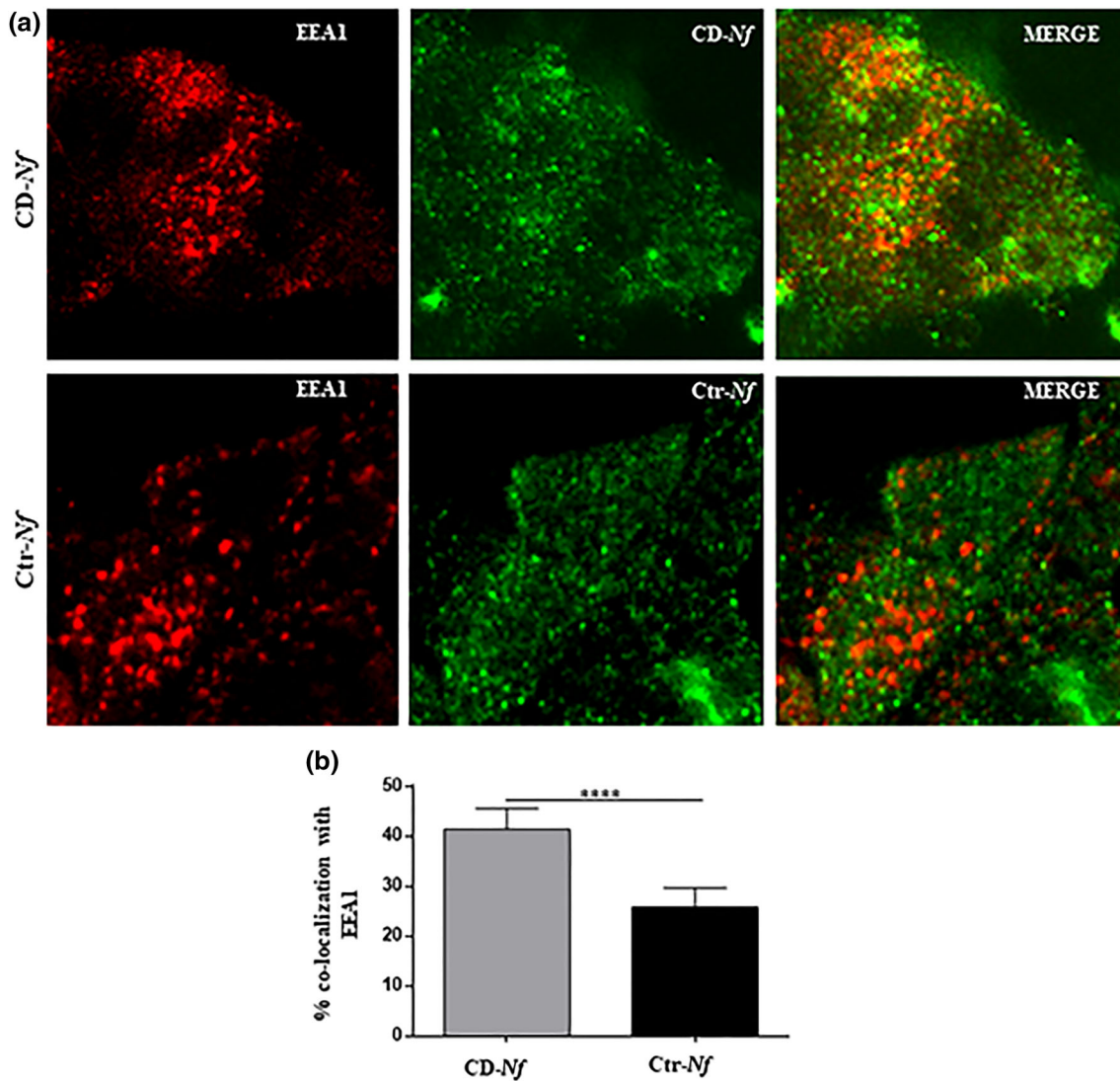
FIGURE 1 Celiac disease (CD)-*Neisseria flavescens* colocalised more with early endosome antigen 1 (EEA1) than control (Ctr)-*N. flavescens*. (a) Fluorescence images of CaCo2 cells infected with CD-*N. flavescens* and Ctr-*N. flavescens*. CD-*N. flavescens* and Ctr-*N. flavescens* are shown in green; EEA1 is shown in red and yellow indicated colocalisation. (b) Statistical analysis of the EEA1/CD-*N. flavescens* or Ctr-*N. flavescens* colocalisation in CaCo-2 cells. The experiments were replicated 9 times. The columns and bars represent the mean and standard deviation. Student's *t* test [****]$P < .0001$

significantly increased ($P < .05$ and $P < .01$, respectively) their colocalisation in the early compartment (Figure 3c,d), thereby globally increasing the *N. flavescens* content in the early compartment. Moreover, the P31-43 peptide significantly increased the level of CD-*N. flavescens* and Ctr-*N. flavescens* in the autophagosomal compartment ($P < .001$ and $P < .05$, respectively; Figure 3e,f).

2.3 | Effect of pretreatment with *L. paracasei*-CBA probiotic supernatant on the entry, viability, and intracellular localisation of CD-*N. flavescens* and Ctr-*N. flavescens* in CaCo-2 cells in the presence and absence of P31-43

We asked whether pretreatment of cells with *L. paracasei*-CBA supernatant could in some way counteract the effect of CD-

associated dysbiosis in CaCo-2 cells, notwithstanding the presence of the P31-43 peptide. The rationale of this experiment was based on several reasons: (a) low levels of *Lactobacilli* have been reported in active CD patients (D'Argenio et al., 2016; Di Cagno et al., 2011; Nadal et al., 2007; Nistal et al., 2012), (b) lower faecal levels of *Lactobacillus* in active CD patients than in controls have been associated with differences in gluten metabolism between the two groups of individuals (Caminero et al., 2015), (c) experimental evidence obtained by our group indicated that the pretreatment of CaCo-2 cells with *L. paracasei*-CBA supernatant reduced the entry of gliadin peptides into the cell, thereby decreasing their toxicity (Sarno et al., 2014),

Using immunofluorescence, we tested whether *L. paracasei*-CBA supernatant could affect the entry of *N. flavescens* bacteria into CaCo-2 cells. As shown in Figure 2a,b CD-*N. flavescens* levels were
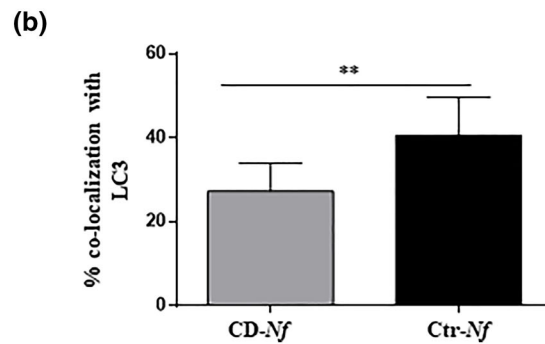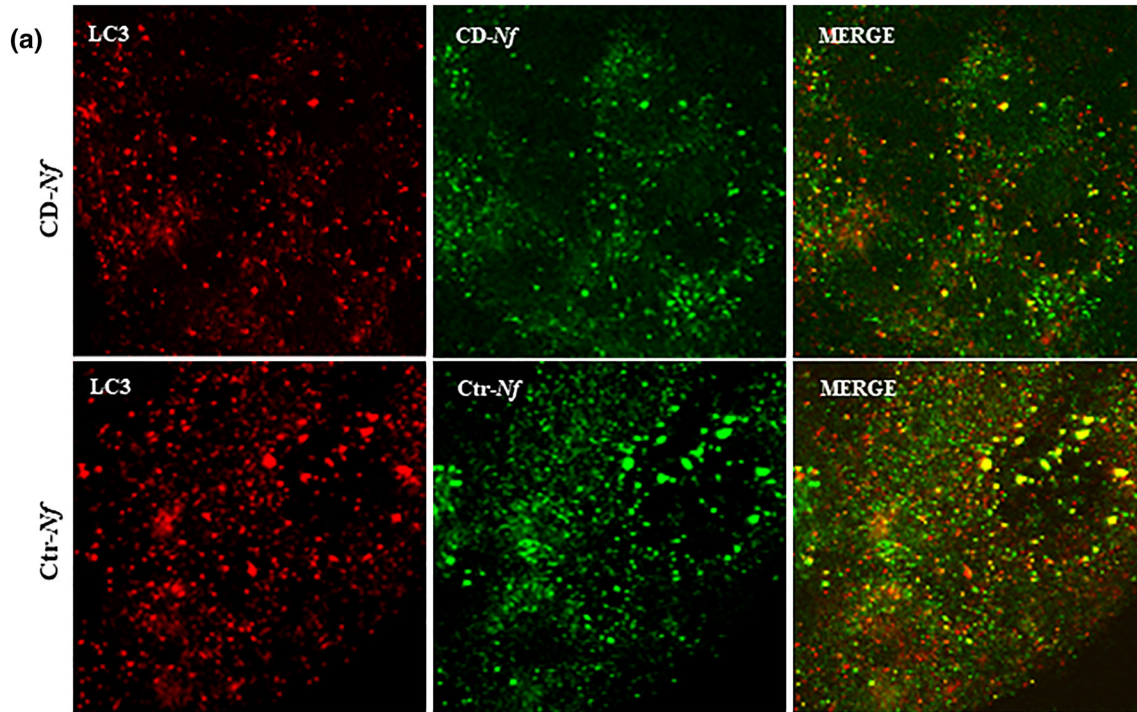
FIGURE 2 Celiac disease (CD)-*Neisseria flavescens* colocalised less with light chain 3B (LC3) than controll (Ctr)-*N. flavescens*. (a) Fluorescence images of CaCo-2 cells infected with CD-*N. flavescens* and Ctr-*N. flavescens*. CD-*N. flavescens* and Ctr-*N. flavescens* are shown in green; LC3 is shown in red and yellow indicated colocalisation. (b) Statistical analysis of the LC3/CD-*N. flavescens* or Ctr-*N. flavescens* colocalisation in CaCo-2 cells. The experiments were replicated 9 times. The columns and bars represent the mean and standard deviation. Student's *t* test [**]$P < .01$

significantly higher than Ctr-*N. flavescens* levels ($P < .05$) in untreated CaCo-2 cells 1 hr after infection. We verified bacteria viability by evaluating viable bacteria count in CaCo-2 *N. flavescens*-infected cell lysates (Figure S2c,d). Notably, the probiotic supernatant did not significantly affect the entry of bacterium into the cells but reduced its viability (Figure S2a–g). Pretreatment with *L. paracasei*-CBA increased the colocalisation of CD-*N. flavescens* with LAMP-2 and decreased the colocation with EEA1 (Figure 4a,c; $P < .01$ and $P < .0001$, respectively) but did not significantly affect intracellular Ctr-*N. flavescens* colocalisation (Figure 4b,d). No change in the intracellular trafficking of *N. flavescens* bacteria was observed after the addition of the P31-43 toxic peptide to CaCo-2 cells pretreated with *L. paracasei*-CBA (Figure 4a–d).

2.4 | Metabolic phenotype of untreated CaCo-2 cells and of *N. flavescens*-infected CaCo-2 cells analysed before and after exposure to various treatments

We previously showed that *N. flavescens* isolated from duodenal and oropharyngeal samples of active CD patients triggered an immune-inflammatory reaction in mucosal duodenal explants and in CaCo-2 cells (D'Argenio et al., 2016). In the present study, we asked if, parallel to the inflammatory response, *N. flavescens* induces changes in the CaCo-2 bioenergetics (measured using an extracellular flux analyser: XF) and thus concurs to exacerbate the epithelial intestinal cell malfunction. To this end, we investigated metabolic phenotypes, in terms of glycolysis and oxidative phosphorylation, in NT and
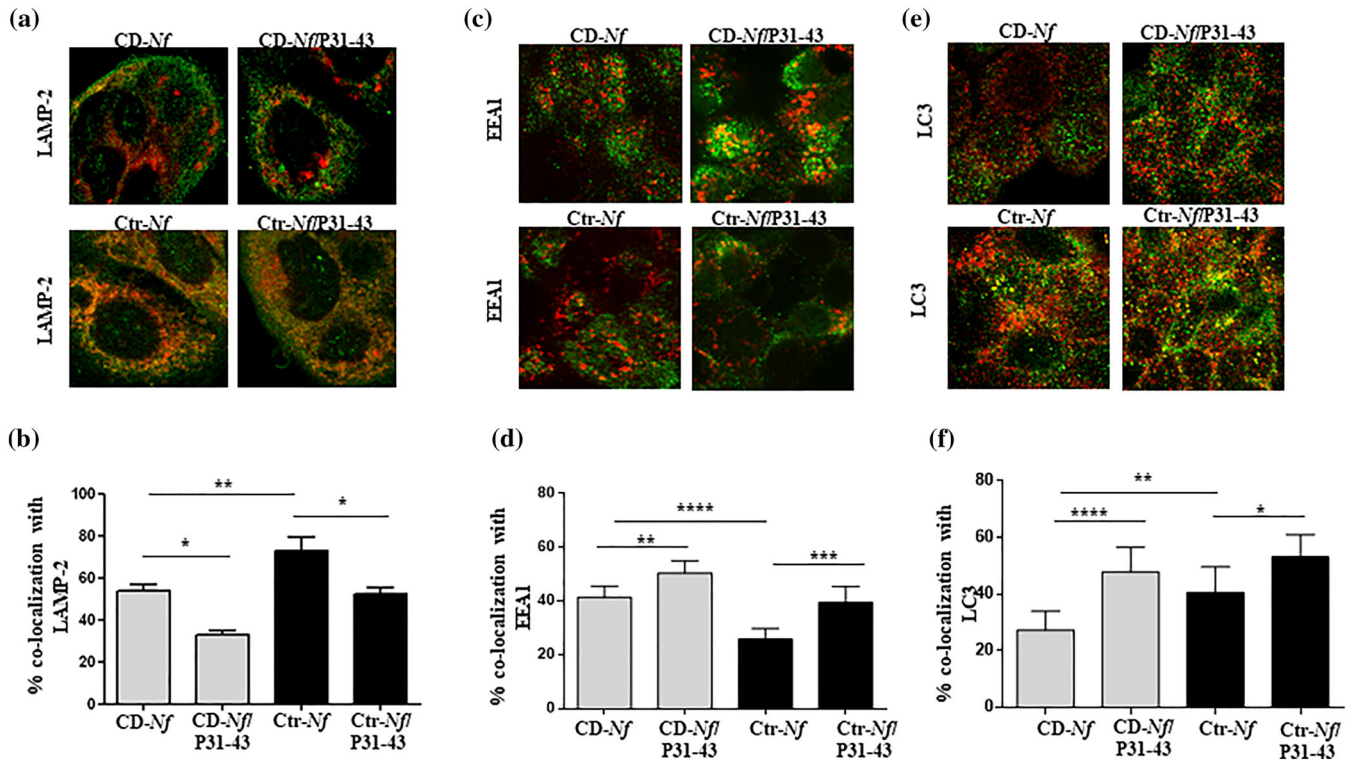
FIGURE 3 P31-43 peptide treatment decreased celiac disease (CD)-*Neisseria flavescens* and control (Ctr)-*N. flavescens* localisation in the late compartment and increased that in the early endosomal and autophagosomal compartments, respectively. Fluorescence images of CaCo-2 cells infected with CD-*N. flavescens* or Ctr-*N. flavescens* after treatment with P31-43. CD-*N. flavescens* and Ctr-*N. flavescens* are shown in green, (a) anti-lysosomal-associated membrane protein-2 (LAMP-2), (c) early endosome antigen 1 (EEA1), and (e) light chain 3B (LC3) are shown in red; yellow indicates colocalisation. Statistical analysis of (b) LAMP-2, (d) EEA1, and (f) LC3 colocalisation of CD-*N. flavescens* and Ctr-*N. flavescens* in CaCo-2 cells after treatment with peptide P31-43. The columns and bars represent mean and standard deviation. The experiments were replicated 6 times (LAMP-2, EEA1) or 4 times (LC3). Student's *t* test $^{*}P < .05$, $^{**}P < .01$, $^{***}P < .001$, $^{****}P < .0001$

CD-*N. flavescens*-infected CaCo-2 cells, and then, the latter were compared with the metabolic phenotypes obtained in CaCo-2 cells after each of the following treatments: pretreatment with *L. paracasei*-CBA, addition of P31-43, CD-*N. flavescens*/P31-43, *L. paracasei*-CBA/CD-*N. flavescens*, or *L. paracasei*-CBA/CD-*N. flavescens*/P31-43 (Figures S3 and 5). Globally, we found that both glycolytic performance and oxidative phosphorylation (an indicator of mitochondrial respiratory capacity) were significantly lower in CD-*N. flavescens*-infected CaCo-2 cells than in either treated or NT cells (*P* < .05; Figure S3a,b). In detail, basal glycolysis, measured by extracellular acidification rate (ECAR; Figure 5a), was lower, albeit not significantly so, in CD-*N. flavescens*-infected CaCo-2 cells than in NT cells (ECAR, Cd-*N. flavescens* = 12.3 ± 1.7 mpH/min vs. NT = 16.5 ± 1.4 mpH/min), whereas it was significantly lower (*P* < .05) in CD-*N. flavescens*-infected cells than in either *L. paracasei*-CBA or *L. paracasei*-CBA/CD-*N. flavescens*/P31-43-treated CaCo-2 cells (ECAR, 23.3 ± 2.3 mpH/min). Moreover, basal glycolysis did not differ between NT and P31-43-treated CaCo-2 cells (ECAR, 17.7 ± 1.3 mpH/min) and was significantly lower in NT than in *L. paracasei*-CBA-treated CaCo-2 cells (ECAR, 22.2 ± 1.4 mpH/min, *P* < .05; Figure 5a).

The glycolytic reserve, which represents the difference between maximal glycolysis post-oligomycin addition and basal glycolysis (Figure 5b), was similar in CD-*N. flavescens*-infected cells and NT cells, whereas it exceeded NT values in CaCo-2 cells exposed to any of the other treatments tested (*P* < .05). Glycolytic capacity, which represents the maximum glycolytic rate, was significantly lower in CD-*N. flavescens*-infected CaCo-2 cells than in NT cells or in cells exposed to any other treatment tested (*P* < .05; Figure S3A).

Mitochondrial activity, which is basal respiration measured by Oxygen Consumption Rate (OCR; Figure 5C), was significantly lower in CD-*N. flavescens*-infected cells than in NT CaCo-2 cells (OCR, CaCo-2/CD-*N. flavescens* = 49.4 ± 1.7 pmol/min, NT = 102.1 ± 1.6 pmol/min, *P* < .05) and in cells exposed to other treatment: *L. paracasei*-CBA (OCR, 82.6 ± 6.3 pmol/min, *P* < .05), P31-43 (OCR, 103.4 ± 1.5 pmol/min, *P* < .05), CD-*N. flavescens*/P31-43 (OCR, 94.2 ± 1.6 pmol/min, *P* < .05), *L. paracasei*-CBA/Cd-*N. flavescens* (OCR, 85.0 ± 2.2 pmol/min, *P* < .05), and *L. paracasei*-CBA/CD-*N. flavescens*/P31-43 (OCR, 74.3 ± 1.8 pmol/min, *P* < .05). Uncoupled mitochondrial activity (i.e., OCR post-FCCP—OCR Ant/Rot) is reported in Figure S4. Spare respiratory capacity (Figure 5d), which represents the difference between maximal
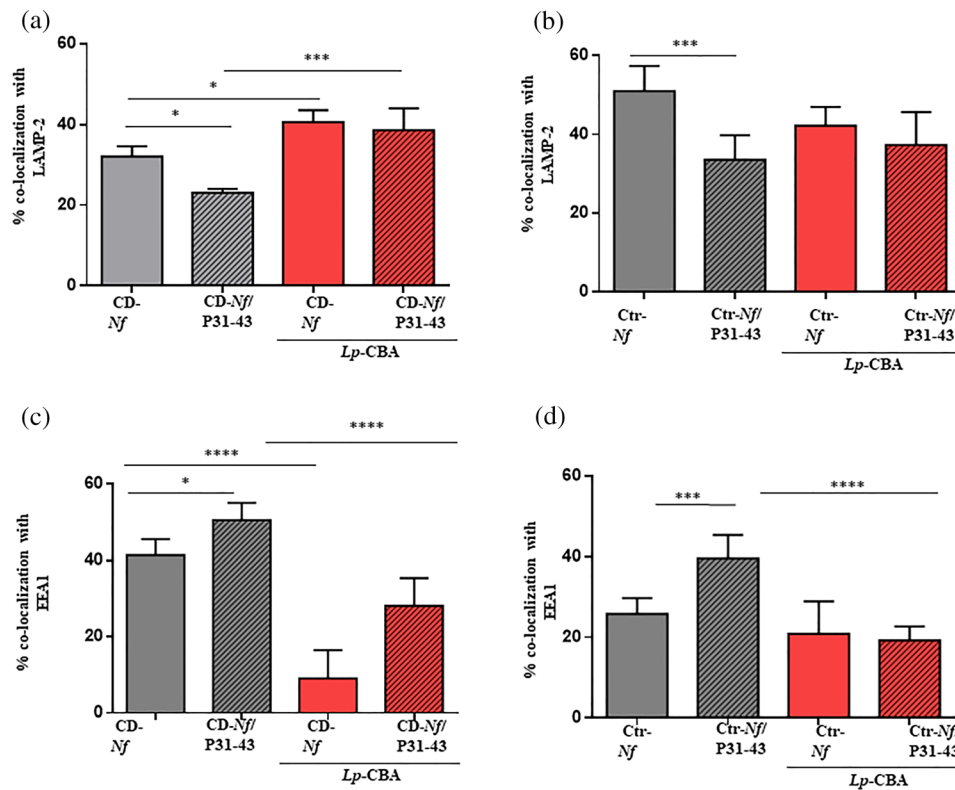
FIGURE 4 *Lactobacillus paracasei* CBA L74 (*L. paracasei*-CBA) increased celiac disease (CD)-*Neisseria flavescens* colocalisation with anti-lysosomal-associated membrane protein-2 (LAMP-2), whereas it reduced that with early endosome antigen 1 (EEA1) in presence of the P31-43 gliadin peptide. Statistical analysis of the colocalisation of CD-*N. flavescens* and control (Ctr)-*N. flavescens* with LAMP-2 (a, b, respectively) and EEA1 (c, d, respectively) in cells pretreated with *L. paracasei*-CBA in the absence and presence of the P31-43 peptide. The columns and bars represent mean and standard deviation. The experiments were replicated 3 times. Student's *t* test [*]$P < .05$, [**]$P < .01$, [***]$P < .001$, [****]$P < .0001$

respiration post-FCCP addition and basal respiration, did not differ among NT, CD-*N. flavescens*-infected and *L. paracasei*-CBA pretreated CaCo-2 cells, whereas it was significantly higher ($P < .05$) in cells treated with the P31-43 immunogenic peptide than in NT cells. Similar results were obtained in Ctr-*N. flavescens*-infected CaCo2 cells (data not shown). We also calculated the ECAR/OCR ratio (Figure 5e), which is an indicator of the relative utilisation of glycolysis and oxidative phosphorylation, in each of the six experimental conditions included in this study and in NT cells. The ECAR/OCR ratio was significantly higher in CD-*N. flavescens*-infected CaCo-2 cells than in NT cells (0.25 ± 0.03 vs. 0.16 ± 0.01 mpH/pmol, $P < .05$). It was also significantly higher in *L. paracasei*-CBA and in *L. paracasei*-CBA/CD-*N. flavescens*/P31-43-treated CaCo2 cells than in NT cells ($P < .05$). On the contrary, the ECAR/OCR ratio did not differ between NT and P31-43-treated cells (Figure 5e).

Globally, our data indicate that, after *N. flavescens* infection, the bioenergetics metabolism in CaCo-2 epithelial cells is less efficient than in NT cells and is characterised by a significant decrease in oxidative phosphorylation activity. This effect was not observed in *N. flavescens*-infected CaCo-2 cells exposed to the P31-43 toxic peptide or in cells pretreated with the *L. paracasei*-CBA supernatant.

2.5 | Measurement of oxidative stress and ATP content in CaCo-2 cells after *N. flavescens* infection and effect of pretreatment with *L. paracasei* supernatant

To quantify oxidative stress in *N. flavescens*-infected cells and to test the efficacy of cellular pretreatment with *L. paracasei*-CBA supernatant in reducing it, we measured malondialdehyde (MDA) level, which is an indicator of cellular oxidative stress. MDA content increased from 3.2 μM in NT CaCo-2 cells up to 10.0 μM in CD-*N. flavescens*-infected CaCo-2 cells, which indicates that bacterial infection caused an increase in cellular oxidative stress (Figure S5). Interestingly, in CaCo-2 cells pretreated with *L. paracasei*-CBA supernatant, cellular stress after CD-*N. flavescens* infection was lower than in NT cells (MDA = 5.8 μM; Figure S5a). These results indicate that the *L. paracasei*-CBA supernatant is able to reduce by about 50% the cellular stress associated with *N. flavescens* infection.

We then evaluated whether the significant decrease in cellular oxidative phosphorylation (mitochondrial activity) caused by the bacterial infection was paralleled by a change in ATP production and whether the pretreatment of cells with *L. paracasei*-CBA supernatant affected
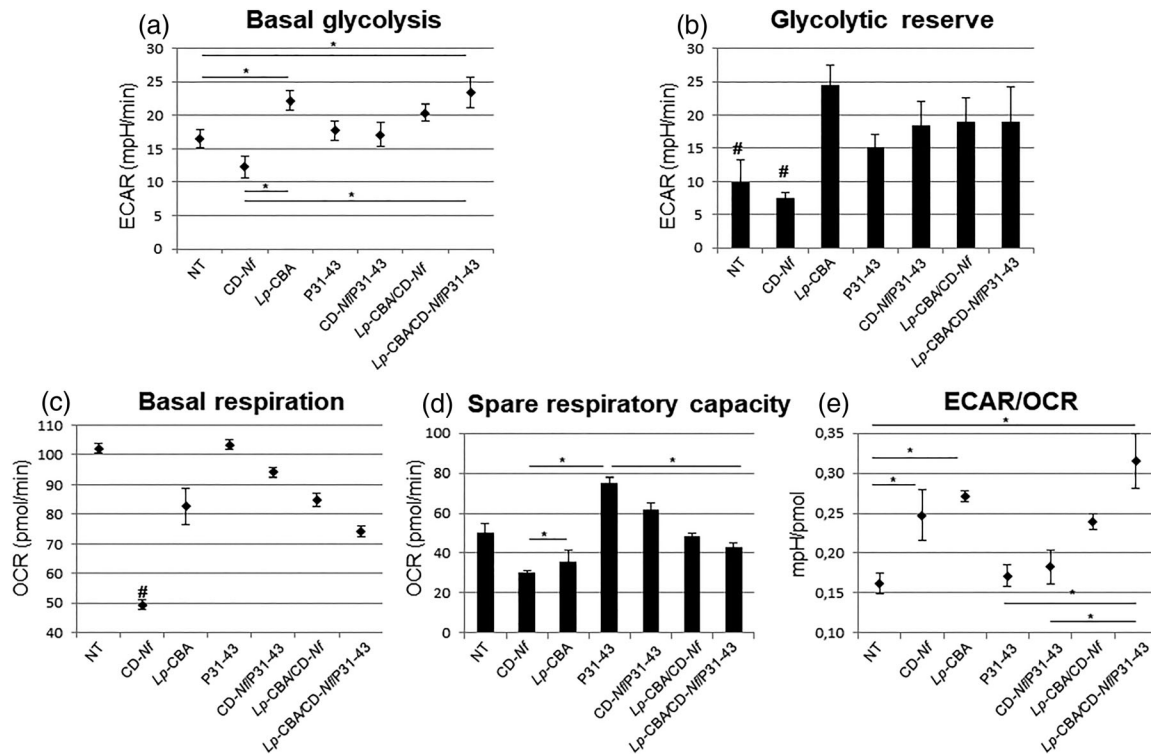
FIGURE 5 Metabolic phenotype of not treated and of differently treated CaCo-2 cells. Bioenergetics profiles in not treated CaCo-2 (NT) cells and in CaCo-2 cells cocultured with: celiac disease (CD)-*Neisseria flavescens*; *Lactobacillus paracasei* CBA L74 (*L. paracasei*-CBA); P31-43 peptide; CD-*N. flavescens*/P31-43; *L. paracasei*-CBA/CD-*N. flavescens*; *L. paracasei*-CBA/CD-*N. flavescens*/P31-43. (a) Basal glycolysis extracellular acidification rate (ECAR; (measured as the difference between post-glucose addition ECAR and non-glycolytic ECAR). (b) Glycolytic reserve (measured as the difference between maximal glycolysis postoligomycin addition and basal glycolysis). (c) Basal respiration oxygen consumption rate (OCR; measured as the difference between preoligomycin addition and nonmitochondrial respiration). (d) Spare respiratory capacity (measured as the difference between maximal respiration post-FCCP addition and basal respiration). (e) ECAR/OCR ratio, a measure of cell relative utilisation of glycolysis and oxidative phosphorylation. Data are expressed as mean ± SEM. Data comparison between groups was performed using the Kruskal–Wallis test. *Statistically significant differences ($P < .05$) after Bonferroni correction between groups encompassed by the bar. #Statistically significant differences ($P < .05$) after Bonferroni correction between the highlighted group and each of the other tested conditions

mitochondrial activity. Therefore, we measured ATP level in NT and in *N. flavescens*-infected CaCo-2 cells pretreated or not with *L. paracasei*-CBA supernatant. The ATP level was 91.1 nM in NT CaCo-2 cells and decreased to 66.4 nM in *N. flavescens*-infected CaCo-2 cells. A similar reduction occurred in *N. flavescens*-infected CaCo-2 cells pretreated with *L. paracasei* CBA supernatant (45.5 nM; Figure S5b). This result suggests that, although the *L. paracasei*-CBA supernatant reduces the viable bacterial load, mitochondrial activity was still damaged and that metabolism probably shifted versus glucose conversion to lactate. Given the low number of samples tested in each experimental condition ($n = 2$), we were unable to obtain a statistically significant difference with the ANOVA test.

3 | DISCUSSION

The aims of this study were to investigate (a) if, parallel to the inflammatory response, the *N. flavescens* strain, which is increased in duodenal and oropharyngeal samples from active celiac patients (D'Argenio

et al., 2016; Iaffaldano et al., 2018), induces changes in the CaCo-2 bioenergetics thus concurring to exacerbate the epithelial intestinal cell malfunction; (b) if the intracellular trafficking of *N. flavescens* and the immunogenic P31-43 peptide could influence each other; and (c) if the pretreatment of CaCo-2 cells with the *L. paracasei*-CBA supernatant could modify the effect of CD-*N. flavescens*-associated dysbiosis on the cell, despite the presence of the P31-43 peptide.

Mitochondrial oxidative phosphorylation was significantly reduced in CD-*N. flavescens*-infected CaCo-2 cells versus NT cells, which together with the significantly increased ECAR/OCR ratio, suggested a shift in CD-*N. flavescens*-infected CaCo-2 cell metabolism towards a more glycolytic phenotype. Glycolysis and mitochondrial oxidative phosphorylation are two important ATP-generating pathways used to meet energy cell demand in physiological conditions (Kramer, Ravi, Chacko, Johnson, & Darley-Usmar, 2014). The metabolic switch from oxidative phosphorylation to glycolysis has been described in various cell types and conditions (Kramer et al., 2014). Notably, it was found to provide ATP and thus to maintain mitochondrial membrane potential in monocyte–macrophage cells during inflammation (O'Neill &

Hardie, 2013). Furthermore, glycolytic reprogramming in the host response to bacteria has been described in *Mycobacterium tuberculosis*-infected murine lungs (Shi et al., 2015) and was found to be required for inflammatory cytokine production (Braverman, Sogi, Benjamin, Nomura, & Stanley, 2016). Hansen et al. (2018) recently described bacteria-induced conversion of a tolerogenic to an inflammatory response in human intestinal CD103^{+} dendritic cells and found that cytokine production depended on glycolytic reprogramming that mediated the upregulation of cytokine translation. Given that *N. flavescens* isolates induce inflammatory cytokine secretion in CaCo-2 cells, and in murine and human CD103^{+} dendritic cells (D'Argenio et al., 2016), it is feasible that glycolytic reprogramming could occur in our experimental epithelial system. Inhibition of oxidative phosphorylation was reported to increase cell production of reactive oxygen species that exert bactericidal activities (O'Neill & Hardie, 2013). In agreement with that finding, we found higher levels of MDA, which is an indicator of cellular stress, in *N. flavescens*-infected CaCo-2 cells than in NT CaCo-2 cells. Alteration of oxidative metabolism was also supported by the decrease in ATP intracellular content in CD-*N. flavescens*-infected CaCo-2 cells versus NT CaCo-2 cells. Consequently, it is likely that *Neisseria* infection induces bactericidal activity in CaCo-2 cells also through this mechanism. In this context, it is interesting to recall that iron perturbation at intestinal epithelial cell level can negatively impact mitochondrial function (Paul, Manz, Torti, & Torti, 2017) and that competition for iron is a key aspect of infectious diseases (Caza & Kronstad, 2013). Consequently, it is tempting to speculate that the genetic differences in the iron acquisition system that we previously demonstrated between CD-associated *N. flavescens* and the Ctr-*N. flavescens* (D'Argenio et al., 2016) could also concur to the mitochondrial dysfunction observed in this study.

Despite the presence of the P31-43 peptide, pretreatment of CaCo-2 cells with *L. paracasei*-CBA supernatant appeared to improve cellular bioenergetics after *N. flavescens*-infection likely due to the probiotic's ability to reduce bacterial viability. Notably, in *L. paracasei*-CBA pretreated CD-*N. flavescens*-infected CaCo-2 cells, we observed the recovery of glycolysis (glycolytic reserve) and only a partial improvement of mitochondrial respiration as shown by the decrease in MDA production but not yet complete recovery of ATP production. In agreement with our data, and in the context of the general balance of cellular energy metabolism, an increase of lactate production was previously observed when cells tried to compensate ATP loss, which is indicative of damaged oxidative metabolism (i.e., respiration; Vander Heiden & De Berardinis, 2017).

The localization experiments of CD-*N. flavescens* and Ctr-*N. flavescens* in intestinal CaCo-2 epithelial cells demonstrated that, after entering the cell, unlike Ctr-*N. flavescens*, the presence of CD-*N. flavescens* was higher in the early endocytic compartment than in the late endocytic compartment, which confirms and extends our previous finding (D'Argenio et al., 2016). Although we observed only modest increases in the presence of the CD-associated *N. flavescens* in the early endocytic compartment, we and others previously showed that similar alterations could influence several cell functions, ranging from proliferation to actin organisation, cell motility, and

stress/innate immunity activation (Barone et al., 2007; Barone et al., 2010; Caldieri, Malabarba, Di Fiore, & Sigismund, 2018; De Matteis & Luini, 2011; Nanayakkara et al., 2013; Nanayakkara et al., 2018; Raiborg, Malerød, Pedersen, & Stenmark, 2008; Scita & Di Fiore, 2010; Siegert et al., 2018; Vicinanza et al., 2011). The intracellular location of CD-*N. flavescens* is in agreement with the finding that pathogenic *Neisseria meningitidis* is internalised and creates a replicative niche within the intracellular membranous vacuoles (Barrile et al., 2015). In addition, as autophagy is a fundamental host response to invasion by a variety of bacterial pathogens (Randow & Youle, 2014), we investigated whether intracellular *N. flavescens* is directed to phagosomes for destruction or whether it eludes autophagy-mediated killing. We observed that CD-*N. flavescens* colocalises less than Ctr-*N. flavescens* with the autophagy marker LC3. This finding indicates that CD-*N. flavescens* escapes the autophagy process, probably by "taking refuge" in the early compartment. Accordingly, *Neissera gonorrhoeae* has recently been reported to escape early autophagy-mediated killing by inhibiting autophagosome maturation and lysosome fusion (Lu et al., 2018). Similar to CD-*N. flavescens* intracellular behaviour was also described in pathogenic *N. meningitidis* and *Neissera gonorrhoeae* (Barrile et al., 2015; Lu et al., 2018). Indeed, by subverting intracellular trafficking, which is one of the main survival mechanisms of human pathogens (Barrile et al., 2015; Sullivan, Young, McCann, & Braunstein, 2012; Zhang et al., 2018), CD-*N. flavescens* is more able to escape killing and survive in intestinal cells than Ctr-*N. flavescens*.

Given the above, we investigated if the addition of the P31-43 toxic gliadin peptide could influence the intracellular trafficking of CD-*N. flavescens* and Ctr-*N. flavescens*. The treatment of *N. flavescens*-infected CaCo-2 cells with the P31-43 peptide increased the colocalisation of *N. flavescens* strains with the EEA1 marker, which confirms that P31-43 can delay vesicular trafficking irrespective of the vesicle cargo. It is conceivable that *N. flavescens* strains and the P31-43 peptide cooperate to delay endocytic trafficking at the level of the early compartment thereby providing a "comfort zone" to enable bacteria to survive longer in the cells. Notably, P31-43 increased the colocalisation of the *N. flavescens* isolates with LC3-positive vesicles, but not with LAMP-2-positive compartments, which suggests that also LC3 vesicles cannot reach the late degradative vesicles. In this context, it is feasible that P31-43 causes LC3 vesicles to increase their fusion with the EEA1-positive compartment (Barone, manuscript in preparation). We also show that, although *L. paracasei*-CBA probiotic supernatant did not alter entry of the bacteria into the cell, it reduced the bacterium viability. Furthermore, *L. paracasei*-CBA probiotic supernatant significantly reduced and increased the colocalisation of CD-*N. flavescens* with EEA1 and with LAMP-2 markers, respectively, despite the presence of the P31-43 peptide. As pretreatment of CaCo-2 epithelial cells with *L. paracasei*-CBA probiotic can prevent entry of the P31-43 gliadin peptide into cells (Sarno et al., 2014), it is likely that this effect also impacts on the intracellular localization of the *N. flavescens* strain. Moreover, alterations of trafficking similar to those we found have been associated with or have been reported to directly cause, changes in signalling pathways (Scita & Di Fiore,

2010; Nanayakkara et al., 2013; Nanayakkara et al. 2018). These earlier findings together with our results may help to shed light on the disease pathology.

In conclusion, the *N. flavescens* strain that we identified in duodenum and oropharyngeal samples from patients with active CD (D'Argenio et al., 2016; Iaffaldano et al., 2018), induces imbalance in the mitochondrial respiration of CaCo-2 epithelial cells in parallel to the inflammation-immune response. This metabolic alteration appears to be in part reversed by the probiotic *L. paracasei*-CBA, irrespective of the presence of the P31-43 peptide. Although our data obtained in cultured cells cannot be extrapolated to the duodenal epithelium, they are compatible with an additional mechanism through which CD-*N. flavescens* could concur to the malfunction of the intestinal epithelium in CD patients and suggests that the *L. paracasei*-CBA probiotic could be used to correct CD-associated dysbiosis.

4 | EXPERIMENTAL PROCEDURES

4.1 | Cellular and bacterial growth conditions

CaCo-2 cells were grown for 5 or 6 days in Dulbecco's modified Eagle's medium (DMEM; GIBCO, San Giuliano Milanese, Italy) supplemented with 10% fetal calf serum (FCS, GIBCO), 100 units/ml of penicillin–streptomycin (GIBCO), and 1-mM glutamine (GIBCO). The medium was changed every 2 days. The *N. flavescens* strains were isolated as previously described (D'Argenio et al., 2016) from the duodenum of CD patients and from the oropharynx of a healthy control subject and were used at a multiplicity of infection of 1:100. We used *L. paracasei*-CBA isolated from the faeces of healthy newborn children and previously tested for its anti-inflammatory capacity (International Depository Accession Number LMG P-24778; Zagato et al., 2014). To prepare the probiotic supernatant, we cultivated *L. paracasei*-CBA L74 in DMEM supplemented with 10% fetal calf serum (FCS, GIBCO), and 1-mM glutamine (GIBCO) until 10^9 CFU/ml as previously described (Sarno et al., 2014). The bacterial culture was then centrifuged at 3,000 rpm for 10 min and the supernatant was filtered through a 0- to 22-micron filter. When required, lipopolysaccharide-free synthetic P31-43 peptides (Inbios, Naples, Italy; >95% pure, evaluated by matrix-assisted laser desorption/ionisation time-of-flight mass spectrometry) were added to cell cultures. The peptides were obtained using Ultrasart-D20 filtration (Sartorius AG, Gottingen, Germany). The level of lipopolysaccharide in these peptides was below the detection threshold (i.e., <0.20 EU/mg), as assessed using the QCL-1000 kit (Cambrex Corporation, NJ, USA). The sequence of P31-43 was LGQQQPFPPQQPY. The peptides were used at a concentration of 100 μg/ml (Nanayakkara et al., 2018).

4.2 | Intracellular localization of *N. flavescens* in CaCo-2 epithelial cells

CaCo-2 cells were seeded on glass coverslips for 2 days. The cells (1×10^5) were then infected with bacteria for 1 hr at MOI 1:100. After treatment with gentamicin (100 μg/ml) for 30 min to kill extracellular bacteria, the coverslips were washed, and 6 hr later, they were fixed with 3% paraformaldeide for 5 min at room temperature and permeabilised with Triton (Biorad, Milan, Italy) 0.2% for 5 min at room temperature. They were then stained for 1 hr at room temperature with rabbit polyclonal anti-*N. meningitidis* antibody (Virostat 6121, BD Pharmigen, Milan, Italy). Secondary antibodies conjugated (Invitrogen, Milan, Italy) anti-rabbit Alexa-488 for Neisseria were added to the coverslips for 1 hr at room temperature. The coverslips were then mounted on glass slides and observed with a confocal microscope (LSM 510 Zeiss, Milan, Italy) to obtain images (Figure S6, point 1); 20–30 cells were observed in each sample. Fluorescence analysis was performed with AIS Zeiss software. Magnification of the micrographs was 63× objective, 2× zoom in all figures.

4.3 | EEA1, LAMP-2 or LC3 immunofluorescence staining

The CaCo-2 cells were infected with the bacteria as described above (Figure S6, point 1). P31-43 was added to the cells during the 6 hr before fixation (Figure S6, point 2). Probiotic supernatant was added before CD-*N. flavescens* or Ctr-*N. flavescens* infection (Figure S6, points 3 and 4). Subsequently, cells were stained for 1 hr at room temperature with anti- EEA1 or LAMP-2 or microtubule-associated proteins 1A/1B LC3 antibodies, and with anti-Neisseria antibodies. Secondary antibodies conjugated anti-rabbit Alexa-488 for Neisseria; anti-goat Alexa-546 (Invitrogen, Milan, Italy) for EEA1; anti-mouse Alexa-546 (Invitrogen, Milan, Italy) for LAMP-2; and anti-mouse Alexa-546 (Invitrogen, Milan, Italy) for LC3 were added to the coverslips for 1 hr at room temperature. The coverslips were then mounted on glass slides and observed with a confocal microscope; 20–30 cells were observed in each sample. Images were examined with a Zeiss LSM 510 laser scanning confocal microscope.

4.4 | Colocalisation analysis

Colocalisation analysis was performed with AIS Zeiss software. Magnification of the micrographs was 63× objective, 2× zoom in all. We used Argon/2 (458, 477, 488, 514 nm), HeNe1 (543 nm), and HeNe2 (633 nm) excitation lasers, which were switched on separately to reduce cross-talk of the three fluorochromes. The green and the red emissions were separated by a dichroic splitter (FT 560) and filtered (515- to 540-nm band-pass filter for green and >610-nm long pass filter for red emission). A threshold was applied to the images to exclude about 99% of the signal found in control images. The weighted colocalisation coefficient represents the sum of intensity of colocalising pixels in Channels 1 and 2 compared with the overall sum of pixel intensities above threshold. This value could be 0 (no colocalisation) or 1 (all pixels colocalise). Bright pixels contribute more than faint pixels. The colocalisation coefficient represents the weighted colocalisation coefficient of Ch1 (red) with

respect to Ch2 (green) for each experiment (Araya et al., 2016; Zimmermann et al., 2014).

4.5 | CaCo-2 bioenergetics profiling by extracellular flux analysis

The ECAR and the OCR, which are indicators of glycolysis and mitochondrial respiration, respectively, were measured using the Seahorse XFe96 extracellular flux analyser (Seahorse Bioscience, Agilent Technologies, Santa Clara, CA, USA), which carries a fluorescent probe. The controls were represented by the cell-free culture medium and by not treated CaCo-2 cells. For each tested experimental condition, cells were plated in three wells on Seahorse 96-well plates 24 hr before the experiment at a density of 8×10^3 cells/well. Immediately before the experiment, medium was replaced as follows: For OCR, we used the XF medium (nonbuffered DMEM medium, containing 10-mM glucose, 2-mM L-glutamine, and 1-mM sodium pyruvate), under basal conditions and in response to 1-µM oligomycin (Olig–ATP synthase inhibitor), 1-µM carbonylcyanide-4-(trifluoromethoxy)-phenylhydrazone (FCCP—mitochondrial uncoupling), and 1-µM antimycin A (ant—complex III inhibitor), and rotenone (Rot—Complex 1 inhibitor); for ECAR, we used the glucose-depleted XF medium in basal condition and in response to 10-mM glucose, 1-µM oligomycin, and 50-mM 2-deoxy-D-glucose (2-DG—glycolysis inhibitor). In basal conditions and after the injection of each stimulant or inhibitor chemical additive, the instrumentation measures changes in oxygen concentration (OCR, pmol/min) and in pH (ECAR, mpH/min) three times (about every 10 min). Based on the average of the three measurements, we calculated for the mitochondrial respiration: basal respiration ($OCR_{pre-Olig} - OCR_{post-Ant/Rot}$) and spare respiratory capacity ($[OCR_{post-FCCP} - OCR_{post-Ant/Rot}]$ – basal respiration); for glycolysis: basal glycolysis ($ECAR_{pre-Olig} - ECAR_{pre-Glucose}$), glycolytic reserve ($[ECAR_{post-Olig} - ECAR_{pre-Glucose}]$ – basal glycolysis). Furthermore, we calculated the ECAR/OCR ratio as cell relative utilisation of glycolysis and oxidative phosphorylation.

4.6 | Measurement of CaCo-2 oxidative status and ATP production

The oxidative stress of CaCo-2 cells was evaluated by measuring the MDA content of cells with a colorimetric method using the TBARS assay kit (Cayman chemical, Ann Arbor, MI, USA) according to the manufacturer's instruction. MDA is the end product of lipid peroxidation, an indicator of oxidative stress in cells, and tissue. ATP was measured with a bioluminescence assay ATP kit (Thermo Fisher Scientific, Waltham, MA USA). Both determinations were performed in duplicate in the following groups of cells: NT CaCo-2 cells, CD-*N. flavescens* infected CaCo-2 cells, *L. paracasei* supernatant pretreated CD-*N. flavescens* infected CaCo-2 cells. Briefly, 2×10^7 cells were collected in duplicate for every tested condition and resuspended in 150-µL PBS before sonication; 100 µL were used for MDA determination, whereas 30 µL were used for ATP measurement, according manufacturer's instructions.

4.7 | Statistical analysis

Data are expressed as mean ± SD or SEM as appropriate. Data comparison between groups was performed using the Kruskal–Wallis test, Student's t test, ANOVA, or χ^2 test, as appropriate. Differences were considered statistically significant with a $P < .05$ after Bonferroni correction. Statistical analyses were carried out with the PASW package for Windows (ver.18; SPSS Inc. Headquarters, Chicago, IL).

CONFLICT OF INTEREST

The authors report no conflict of interest.

FINANCIAL DISCLOSURE

KraftHeinz did not provide any financial support to the authors or to the project. The authors report no financial interest or benefit arising from the direct application of this work.

ORCID

Giuseppe Labruna 🄳 https://orcid.org/0000-0002-4436-846X

REFERENCES

Araya, R. E., Gomez Castro, M. F., Carasi, P., McCarville, J. L., Jury, J., Mowat, A. M., … Chirdo, F. G. (2016). Mechanisms of innate immune activation by gluten peptide p31-43 in mice. *American Journal of Physiology. Gastrointestinal and Liver Physiology*, *311*(1), G40–G49. https://doi.org/10.1152/ajpgi.00435.2015

Barone, M. V., Gimigliano, A., Castoria, G., Paolella, G., Maurano, F., Paparo, F., … Auricchio, S. (2007). Growth factor-like activity of gliadin, an alimentary protein: Implications for coeliac disease. *Gut*, *56*(4), 480–488. https://doi.org/10.1136/gut.2005.086637

Barone, M. V., Nanayakkara, M., Paolella, G., Maglio, M., Vitale, V., Troiano, R., … Auricchio, S. (2010). Gliadin peptide P31-43 localises to endocytic vesicles and interferes with their maturation. *PLoS ONE*, *5*, e12246. https://doi.org/10.1371/journal.pone.0012246

Barone, M. V., Troncone, R., & Auricchio, S. (2014). Gliadin peptides as triggers of the proliferative and stress/innate immune response of the celiac small intestinal mucosa. *International Journal of Molecular Sciences*, *15*(11), 20518–20537. https://doi.org/10.3390/ijms151120518

Barone, M. V., & Zimmer, K. P. (2016). Endocytosis and transcytosis of gliadin peptides. *Molecular and Cellular Pediatrics*, *3*(1), 8. https://doi.org/10.1186/s40348-015-0029-z

Barrile, R., Kasendra, M., Rossi-Paccani, S., Merola, M., Pizza, M., Baldari, C., … Aricò, B. (2015). *Neisseria meningitidis* subverts the polarized organization and intracellular trafficking of host cells to cross the epithelial barrier. *Cellular Microbiology*, *17*(9), 1365–1375. https://doi.org/10.1111/cmi.12439

Braverman, J., Sogi, K. M., Benjamin, D., Nomura, D. K., & Stanley, S. A. (2016). HIF-1α is an essential mediator of IFN-γ-dependent immunity to Mycobacterium tuberculosis. *Journal of Immunology*, *197*(4), 1287–1297. https://doi.org/10.4049/jimmunol.1600266

Caldieri, G., Malabarba, M. G., Di Fiore, P. P., & Sigismund, S. (2018). EGFR Trafficking in Physiology and Cancer. *Progress in Molecular and Subcellular Biology*, *57*, 235–272. https://doi.org/10.1007/978-3-319-96704-2_9

Caminero, A., Nistal, E., Herrán, A. R., Pérez-Andrés, J., Ferrero, M. A., Vaquero Ayala, L., & Casqueiro, F. J. (2015). Differences in gluten metabolism among healthy volunteers, coeliac disease patients and first-degree relatives. *The British Journal of Nutrition*, *114*, 1157–1167. https://doi.org/10.1017/S0007114515002767

Caza, M., & Kronstad, J. W. (2013). Shared and distinct mechanisms of iron acquisition by bacterial and fungal pathogens of humans. *Frontiers in Cellular and Infection Microbiology*, *3*(80), 1–15.

Comino, I., Real, A., Gil-Humanes, J., Pistón, F., de Lorenzo, L., Moreno Mde, L., ... Sousa, C. (2012). Significant differences in coeliac immunotoxicity of barley varieties. *Molecular Nutrition & Food Research*, *56*(11), 1697–1707. https://doi.org/10.1002/mnfr.201200358

D'Argenio, V., Casaburi, G., Precone, V., Pagliuca, C., Colicchio, R., Sarnataro, D., ... Sacchetti, L. (2016). Metagenomics reveals dysbiosis and a potentially pathogenic *N. flavescens* strain in duodenum of adult celiac patients. *The American Journal of Gastroenterology*, *111*(6), 879–890. https://doi.org/10.1038/ajg.2016.95

De Matteis, M. A., & Luini, A. (2011). Mendelian disorders of membrane trafficking. *The New England Journal of Medicine*, *365*, 927–938. https://doi.org/10.1056/NEJMra0910494

Di Cagno, R., De Angelis, M., De Pasquale, I., Ndagijimana, M., Vernocchi, P., Ricciuti, P., ... Gobbetti, M. (2011). Duodenal and faecal microbiota of celiac children: Molecular, phenotype and metabolome characterization. *BMC Microbiology*, *11*, 219. https://doi.org/10.1186/1471-2180-11-219

Girbovan, A., Sur, G., Samasca, G., & Lupan, I. (2017). Dysbiosis a risk factor for celiac disease. *Medical Microbiology and Immunology*, *206*(2), 83–91. https://doi.org/10.1007/s00430-017-0496-z

Hansen, I. S., Krabbendam, L., Bernink, J. H., Loayza-Puch, F., Hoepel, W., van Burgsteden, J. A., ... den Dunnen, J. (2018). FcαRI co-stimulation converts human intestinal CD103+ dendritic cells into pro-inflammatory cells through glycolytic reprogramming. *Nature Communications*, *9*(1), 863. https://doi.org/10.1038/s41467-018-03318-5

Iaffaldano, L., Granata, I., Pagliuca, C., Esposito, M. V., Casaburi, G., Salerno, G., ... Sacchetti, L. (2018). Oropharyngeal microbiome evaluation highlights *Neisseria* abundance in active celiac patients. *Scientific Reports*, *8*(1), 11047. https://doi.org/10.1038/s41598-018-29443-1

Kho, Z. Y., & Lal, S. K. (2018). The human gut microbiome—A potential controller of wellness and disease. *Frontiers in Microbiology*, *9*, 1835. https://doi.org/10.3389/fmicb.2018.01835

Kramer, P. A., Ravi, S., Chacko, B., Johnson, M. S., & Darley-Usmar, V. M. (2014). A review of the mitochondrial and glycolytic metabolism in human platelets and leukocytes: Implications for their use as bioenergetic biomarkers. *Redox Biology*, *2*, 206–210. https://doi.org/10.1016/j.redox.2013.12.026

Lu, P., Wang, S., Lu, Y., Neculai, D., Sun, Q., & van der Veen, S. (2018). A subpopulation of intracellular *Neisseria* gonorrhoeae escapes autophagy-mediated killing inside epithelial cells. *The Journal of Infectious Diseases*, *219*(1), 133–144. https://doi.org/10.1093/infdis/jiy237

Marsh, M. N. (1992). Gluten, major histocompatibility complex, and the small intestine. A molecular and immunobiologic approach to the spectrum of gluten sensitivity ('celiac sprue'). *Gastroenterology*, *102*(1), 330–354. https://doi.org/10.1016/0016-5085(92)91819-P

Nadal, I., Donat, E., Ribes-Koninckx, C., Calabuig, M., & Sanz, Y. (2007). Imbalance in the composition of the duodenal microbiota of children with coeliac disease. *Journal of Medical Microbiology*, *56*, 1669–1674. https://doi.org/10.1099/jmm.0.47410-0

Nanayakkara, M., Lania, G., Maglio, M., Auricchio, R., De Musis, C., Discepolo, V., ... Barone, M. V. (2018). P31-43, an undigested gliadin peptide, mimics and enhances the innate immune response to viruses and interferes with endocytic trafficking: A role in celiac disease. *Scientific Reports*, *8*(1), 10821. https://doi.org/10.1038/s41598-018-28830-y

Nanayakkara, M., Lania, G., Maglio, M., Discepolo, V., Sarno, M., Gaito, A., ... Barone, M. V. (2013). An undigested gliadin peptide activates innate immunity and proliferative signaling in enterocytes, the role in celiac disease. *The American Journal of Clinical Nutrition*, *98*, 1123–1135. https://doi.org/10.3945/ajcn.112.054544

Nistal, E., Caminero, A., Herrán, A. R., Arias, L., Vivas, S., de Morales, J. M., ... Casqueiro, J. (2012). Differences of small intestinal bacteria populations in adults and children with/without celiac disease: Effect of age, gluten diet, and disease. *Inflammatory Bowel Diseases*, *18*(4), 649–656.

O'Neill, L. A., & Hardie, D. G. (2013). Metabolism of inflammation limited by AMPK and pseudo-starvation. *Nature*, *493*(7432), 346–355. https://doi.org/10.1038/nature11862

Paul, B. T., Manz, D. H., Torti, F. M., & Torti, S. V. (2017). Mitochondria and iron: Current questions. *Expert Review of Hematology*, *10*, 65–79. https://doi.org/10.1080/17474086.2016.1268047

Raiborg, C., Malerød, L., Pedersen, N. M., & Stenmark, H. (2008). Differential functions of HRS and ESCRT proteins in endocytic membrane trafficking. *Experimental Cell Research*, *314*, 801–813. https://doi.org/10.1016/j.yexcr.2007.10.014

Randow, F., & Youle, R. J. (2014). Self and nonself: How autophagy targets mitochondria and bacteria. *Cell Host & Microbe*, *15*(4), 403–411. https://doi.org/10.1016/j.chom.2014.03.012

Sarno, M., Lania, G., Cuomo, M., Nigro, F., Passannanti, F., Budelli, A., ... Nanayakkara, M. (2014). *Lactobacillus paracasei* CBA L74 interferes with gliadin peptides entrance in Caco-2 cells. *International Journal of Food Sciences and Nutrition*, *65*(8), 953–959. https://doi.org/10.3109/09637486.2014.940283

Scita, G., & Di Fiore, P. P. (2010). The endocytic matrix. *Nature*, *463*(7280), 464–473. https://doi.org/10.1038/nature08910

Shan, L., Molberg, Ø., Parrot, I., Hausch, F., Filiz, F., Gray, G. M., ... Khosla, C. (2002). Structural basis for gluten intolerance in celiac sprue. *Science*, *297*(5590), 2275–2279. https://doi.org/10.1126/science.1074129

Shi, L., Salamon, H., Eugenin, E. A., Pine, R., Cooper, A., & Gennaro, M. L. (2015). Infection with Mycobacterium tuberculosis induces the Warburg effect in mouse lungs. *Scientific Reports*, *5*, 18176.

Siegert, A. M., Serra-Peinado, C., Gutiérrez-Martínez, E., Rodríguez-Pascual, F., Fabregat, I., & Egea, G. (2018). Altered TGF-β endocytic trafficking contributes to the increased signaling in Marfan syndrome. *Biochimica et Biophysica Acta - Molecular Basis of Disease*, *1864*(2), 554–562. https://doi.org/10.1016/j.bbadis.2017.11.015

Sollid, L. M. (2000). Molecular basis of celiac disease. *Annual Review of Immunology*, *18*, 53–81. https://doi.org/10.1146/annurev.immunol.18.1.53

Sullivan, J. T., Young, E. F., McCann, J. R., & Braunstein, M. (2012). The *Mycobacterium tuberculosis* SecA2 system subverts phagosome maturation to promote growth in macrophages. *Infection and Immunity*, *80*(3), 996–1006. https://doi.org/10.1128/IAI.05987-11

Vander Heiden, M. G., & De Berardinis, R. J. (2017). Understanding the intersections between metabolism and cancer biology. *Cell*, *168*, 657–669. https://doi.org/10.1016/j.cell.2016.12.039

Vicinanza, M., Di Campli, A., Polishchuk, E., Santoro, M., Di Tullio, G., Godi, A., ... De Matteis, M. A. (2011). OCRL controls trafficking through early endosomes via PtdIns4,5P$_2$-dependent regulation of

endosomal actin. *The EMBO Journal*, *30*(24), 4970–4985. https://doi.org/10.1038/emboj.2011.354

Zagato, E., Mileti, E., Massimiliano, L., Fasano, F., Budelli, A., Penna, G., & Rescigno, M. (2014). *Lactobacillus paracasei* CBA L74 metabolic products and fermented milk for infant formula have anti-inflammatory activity on dendritic cells in vitro and protective effects against colitis and an enteric pathogen in vivo. *PLoS ONE*, *9*(2), e87615. https://doi.org/10.1371/journal.pone.0087615

Zhang, L., Hu, W., Cho, C. H., Chan, F. K., Yu, J., Fitzgerald, J. R., ... Wu, W. K. (2018). Reduced lysosomal clearance of autophagosomes promotes survival and colonization of *Helicobacter pylori*. *The Journal of Pathology*, *244*(4), 432–444. https://doi.org/10.1002/path.5033

Zimmermann, C., Rudloff, S., Lochnit, G., Arampatzi, S., Maison, W., & Zimmer, K. P. (2014). Epithelial transport of immunogenic and toxic gliadin peptides in vitro. *PLoS ONE*, *9*(11), e113932. https://doi.org/10.1371/journal.pone.0113932

SUPPORTING INFORMATION

Additional supporting information may be found online in the Supporting Information section at the end of the article.